Desalination and Water Treatment
www.deswater.com

doi: 10.5004/dwt.2018.23056

132 (2018) 99–108
November

W/O HIPEs templated polyaniline/polystyrene porous adsorbent for Sr^{2+} uptake from aqueous solution

Yongfeng Zhu[a], Huifang Zhang[b], Xiushen Ye[b], Aiqin Wang[a,*]

[a]*Center of Eco-material and Green Chemistry, Key Laboratory of Clay Mineral Applied Research of Gansu Province, Lanzhou Institute of Chemical Physics, Chinese Academy of Sciences, Tianshui Middle Road 18, Lanzhou, 730000, China, email: zhuyf851013@163.com (Y. Zhu), Tel. +86 931 4968118, Fax +86 931 8277088, email: aqwang@licp.cas.cn (A. Wang),*
[b]*Key Laboratory of Comprehensive and Highly Efficient Utilization of Salt Lake Resources, Qinghai Institute of Salt Lakes, Chinese Academy of Sciences, Xining, 810008, China, email: zhf233007@126.com (H. Zhang), yexs@isl.ac.cn (X. Ye)*

Received 17 January 2018; Accepted 1 September 2018

ABSTRACT

The porous polymer materials have recently received considerable attention as a kind of highly efficient adsorbents. In order to reach the high adsorption capacity, fast adsorption rate and easy of separation, a novel monolithic porous polyaniline/polystyrene (PANI/PS) composite adsorbent was prepared in this study by coating PANI onto the porous PS that was obtained by polymerizing the continuous phase of W/O high internal phase emulsions (HIPEs). The FTIR analysis indicated that the anilino group was loaded onto the porous PS. The SEM images revealed that the as-prepared monolithic adsorbents possessed open-cellular framework structure and PANI was homogenously dispersed onto the PS surface. Subsequently, the porous adsorbent was used to remove Sr^{2+} from aqueous solution. The effects of pH, contact time and initial concentration on the adsorption performance for Sr^{2+} were systematically studied. The results showed that PANI/PS composite can reach equilibrium within 30 min and the maximal adsorption capacity was determined to be 58.85 mg/g. Besides, the PANI/PS monolithic adsorbent showed no significant losses in sorption efficiency even after six cycles of adsorption-desorption, were an indication of its excellent reusability.

Keywords: Porous material; W/O HIPEs; Polyaniline; Adsorbent; Sr^{2+}

1. Introduction

Strontium (Sr) and its compounds are used in many advanced technique field, such as tissue engineering [1], pharmaceuticals [2], military stealth technique [3], electric energy storage materials [4], catalysts [5] and so on. But if the Sr^{2+} enter the environment, especially the major radioactive isotopes, strontium (^{90}Sr), it will generate the most negative effects for aquatic organisms and ultimately cause harm to humans, which has similar properties to calcium and can easily replace it in the human body to induce cancer and some other diseases [6–8]. With the concerns of environmental protection and the economic efficiency, the extraction of Sr^{2+} from wastewater can not only resolve the environmental problem, but also reap significant economic rewards.

The separation and removal of Sr^{2+} from aqueous media by various methods has been previously introduced, including solvent extraction [9], ion exchange [10] and membrane process [11]. But these processes have several disadvantages, including incomplete removal, low selectivity, high operational cost and generation of a large amount of toxic sludge. In addition to these methods, adsorption by solid materials is regarded as the most potential method, because of its simple operation, fast response, relatively low cost and high efficiency [12]. In order to find the most effective Sr^{2+} adsorbent, many inorganic materials (such as sericite [13], zeolite [14], titanate nanotubes [15], manganese antimonate [16] etc.) and organic inorganic hybrid materials (such as covalent triazine polymer–Fe_3O_4 nanocomposite [17], polypyrrole coated nickel oxide nano-particles etc. [18]) have been studied. Unfortunately, the application of functionalized materials as adsorbents also encounter technique problem, due to many of them have tiny particle size and superior

*Corresponding author.

dispersibility in solution. These problems will limit their further utility in industrial processes. Alternatively, the bottleneck of nanoparticle adsorbent can be overcame by the development of monolithic porous adsorbent.

In the matrix of porous adsorbent, the small molecules can be trapped within the mesopores and micropores by an impregnation process, while the macropores are favorable to mass transport process and the micropores make a contribution to specific surface area [19]. Thus, a unique porous structure is critical for rapid diffusion of target molecules into internal surface of the porous adsorbent while enabling efficient adsorption for removal or enrichment the target adsorbate [20–22]. Among of the methods for producing the porous materials with a well-defined porosity, such as hydrothermal synthesis [23], porogenic solvent [24] or sacrificial hard template [25], the emulsion templating is a versatile technology [26]. The porous polymer is obtained by polymerizing the continuous phase of high internal phase emulsions (HIPEs) that contains more than 74.05% of internal phase [27]. Recently, the porous adsorbents prepared from HIPEs have been used to remove or enrich the heavy metals [28–30], rare-earth metals [31], organic pollutants [32,33] and so on, and the porous adsorbents display an excellent adsorption performance.

Polyaniline (PANI), as one of the nitrogen-containing conductive polymer, has been used as the adsorbent for removal of organic and inorganic pollutants due to the advantages of easy synthesis, good environmental stability, and large amounts of amine and imine functional groups [34–37]. However, the PANI is difficult to separate from the treated water via traditional centrifugation and filtration for recycling owing to the small size, as well as the time-consuming and uneconomic process [38]. So the PANI is usually coated onto other matrix material to obtain a composite adsorbent for removal and enrichment of heavy metal, dye and so on [39–43].

In this study, a novel monolithic porous adsorbent for Sr^{2+} removal was prepared by coating the PANI onto the porous polystyrene (PS). The porous substrate of interconnected macroporous sulfated polystyrene was constructed via the W/O high internal-phase emulsions (HIPEs). In order to increase the covering amount of PANI onto the porous PS, the as-prepared porous PS was sulfated prior to the coating process. The preparation process of porous adsorbent is shown in Fig. 1. Then, the adsorption efficiency of monolithic porous adsorbent for Sr^{2+} was systematically studied. Finally, the reusability of this porous adsorbent was also evaluated.

2. Materials and methods

2.1. Materials

Aniline (ANI, A.R. grade), azodiisobutyronitrile (AIBN, A.R. grade), ammonium persulphate (APS, A.R. grade), strontium chloride ($SrCl_2$, A.R. grade) were received from Sinopharm Chemical Reagent Co. Ltd (Shanghai, China). Styrene (St, C.P. grade) and divinyl benzene (DVB, 80%) were all purchased from Kemiou Chemical Reagent Co., Ltd (Tianjin, China). Polyglycerol polyricinoleate (PGPR, B.C. grade) was obtained from Shanghai Woo Industrial Co., Ltd. (Shanghai, China). Other reagents were all analytical grade and all solutions were prepared with distilled water.

2.2. Preparation of porous PS

The porous PS was prepared via the W/O HIPEs. Typically, 3 mL mixture of St and DVB (V_{St}/V_{DVB} = 2/1) and

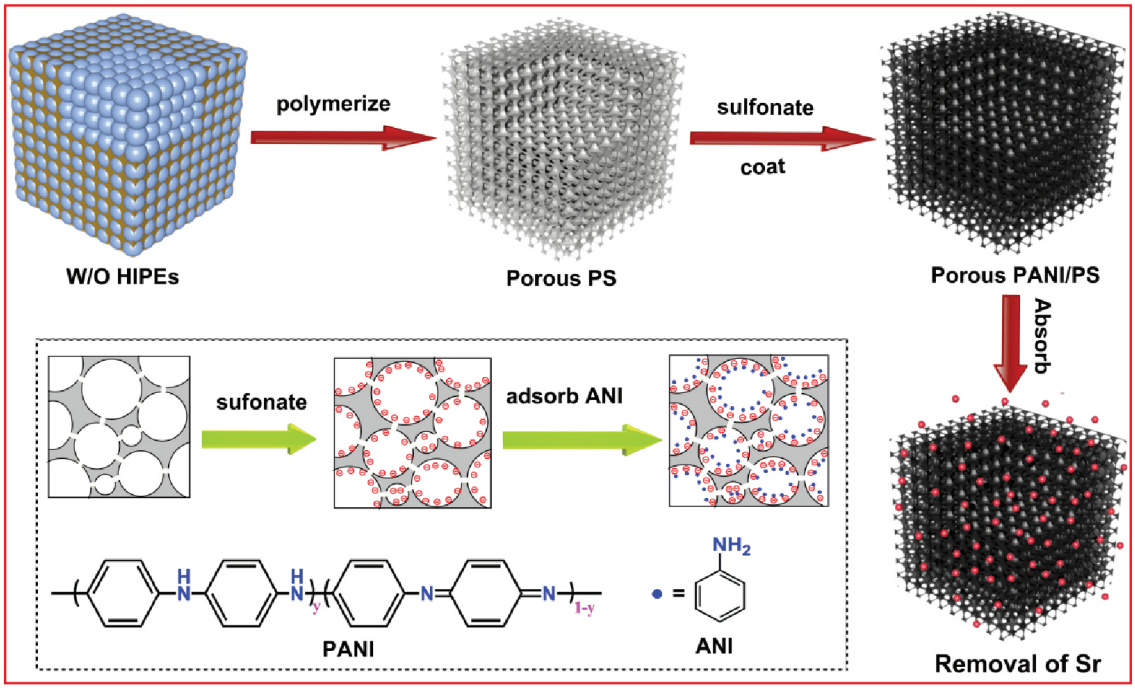

Fig. 1. Preparation of the porous PANI/PS for removal of the Sr^{2+}.

2 g PGPR were stirred together in a 100 mL three-necked flask, 9 mL of distilled water was added dropwise under the vigorous stirring (700 rpm). Then the milky emulsion was formed and the stirring at 700 rpm continued for 2 h, followed by adding 0.1 g of AIBN and stirring for another 3 min at 20 rpm. The viscous emulsion was transferred into plastic tank, sealed and immersed into 70°C water bath and kept for 24 h. The resulting monolith was washed with acetone for 24 h via Soxhlet extraction to remove the surfactant and residual monomer. Afterward, the resulting monolith was cut into slices and dried at 60°C for 12 h under vacuum.

2.3. Preparation of PANI/PS porous adsorbent

The porous adsorbent of PANI/PS was formed by coating PANI onto the porous substrate of PS. In order to enhance the coating effect of PANI onto the porous PS, the porous PS was sulfonated firstly in the concentrated sulphuric acid. Briefly, 0.1 g of porous PS was immersed into 40 mL of concentrated sulphuric acid and stirred for 12 h at 40°C. The product was separated and washed with distilled water for several times, and then dried at 60°C in an oven to the constant weight. After that, 0.3 g of sulfonated porous PS was placed in a mixing solution of alcohol and H_2O solution ($V_{alcohol}/V_{H_2O}$ = 1/1) containing an appropriate amount of aniline for 4 h to achieve the complete adsorption process. Afterward, the oxidation and polymerization of ANI was initiated by using APS solution with APS/ANI molar ratio of 0.5/1. This process was maintained for 20 h at room temperature. The resulting green PANI/PS composite porous was washed thoroughly with distilled water until the supernatant became colorless. Finally, the product was washed with industrial alcohol and dried at room temperature.

2.4. Characterization

The structures of PS and PANI/PS porous adsorbent were analyzed by FTIR spectra (Nicolet NEXUS FTIR spectrometer) in the wave number region of 4000–400 cm^{-1} using KBr pellets. The surface morphologies of monolithic PS, sulfonated PS and PANI/PS were characterized by Field Emission Scanning Electron Microscope (FE-SEM, JSM-6701F, JEOL) after coating the samples with gold film. The pore size distribution was estimated by counting 200 pores using Image Pro Plu as the software tool providing the number distribution of pores. The X-ray photoelectron spectroscopy (XPS) data was obtained with an ESCALab220i-XL electron spectrometer from VG Scientific using 300 W Al Kα radiation.

2.5. Batch adsorption studies

The adsorption experiment was performed by contacting 25 mL of Sr^{2+} solution with 20 mg porous PANI/PS in 50 mL of plastic bottle in the thermostatic oscillator (SHA-C, Changzhou Guohua Co., Ltd., China) for a given time at indoor temperature condition. Then the adsorbent was filtered and the residual concentration of Sr^{2+} solution was determined via the atomic absorption spectroscopy (AAS, TAS-990 Super, Beijing Purkinje General Instrument Co., Ltd). The effects of the initial concentration, contact time, solution pH were all systematically analyzed. The effect of the initial concentration on Sr^{2+} adsorption was studied with the concentration range from 0 to 500 mg/L. The adsorption rate was evaluated at different adsorption time interval ranging from 5 min to 180 min. The effect of pH on the adsorption capacity was analyzed in the Sr^{2+} solution with the pH range from 1.0 to 10.0. The reusability of PANI modified porous PS was investigated via six consecutive adsorption-desorption cycles. The Sr^{2+}-loaded PANI/PS porous adsorbent was desorbed using 0.5 mol/L HCl solution and generated subsequently with 0.5 mol/L NaOH solution. The adsorption capacity of the adsorbent for Sr^{2+} (Q_e) can be calculated by Eq. (1):

$$Q_e = (C_0 - C_e) \times V / m \quad (1)$$

where C_0 and C_e were the initial concentration and the equilibrium concentration of Sr^{2+} (mg/L), V was the volume of solution used (25 mL) and m was the mass of adsorbent used (20 mg).

3. Results and discussion

3.1. Characterization of PANI/PS porous adsorbent

The porous PANI/PS adsorbent was prepared by coating the PANI onto the surface of PS. The PANI layer was formed in the PS by the in-situ free radical polymerization. In order to verify the formation of porous PS, the sulfonation reaction and the coating of the PANI, the FTIR spectra of PS, sulfonated PS and the PANI/PS were given in Fig. 2. In the FTIR spectra of PS, the peak at 3025 cm^{-1} was the C-H stretching vibration of benzene ring. The peaks at 1453 cm^{-1}, 1493 cm^{-1}, and 1601 cm^{-1} were the characteristic bands of C-C stretching vibration of benzene ring [44]. The peaks at 758 cm^{-1} and 700 cm^{-1} were the bands of aromatic C-H out-of-plan bending vibration. The peak at 2925 cm^{-1} belonged to the C-H stretching vibration on the main PS chain. For the sulfonated PS, the peak at the 3422 cm^{-1} was associated with the OH stretching vibration of H_2O [45]. The peak at 1033 cm^{-1} was related to sulfuric acid group ($–SO_3H$) of PS layer. After the coating and polymerization reaction, the new peaks located at 1127 cm^{-1}, 1297 cm^{-1}, 1498 cm^{-1} and 1597 cm^{-1} were related to the vibration band of the dopant anion (HCl-PANI), the C-N stretching mode in Ar-N and the stretching vibration mode of C = C in quinoid rings,

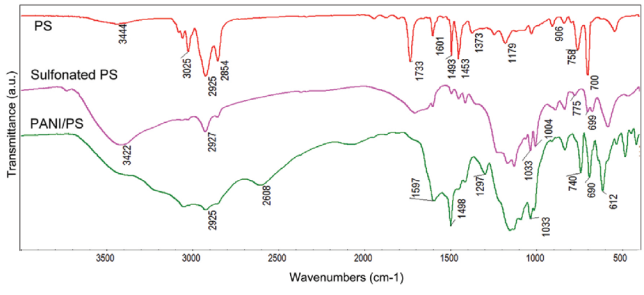

Fig. 2. FT-IR spectra of PS, sulfonated PS and PANI/PS.

C = C in benzenoid rings of PANI appeared in the PANI/PS [46,47]. All the above peaks suggested that the porous PS had been successfully sulfonated and the PANI had been coated onto the sulfonated porous PS.

The morphologies of porous PS and PANI/PS were observed via the SEM (Fig. 3). The monolithic PS showed a homogeneous pore structure, with the average pore size of 7.38 μm. The honeycombed monolith consisted of abundant cellular macrospores and windows (smaller interconnecting pores). The macrospore of open-cellular porous structure was derived from the size of emulsion droplets prior to polymerization and the window was formed upon the rupture of polymer film at its thinnest point. After the sulfonation reaction, the average pore size decreased to 1.37 μm. The pore size distribution became narrow and some pores had been closed. It was caused by the swelling of sulfonated PS in solution. When the ANI molecules diffused into the pore structure of PS, the ANI will be adsorbed onto the surface of porous PS due to the electrostatic interaction between the anilino group and sulfo group. After the polymerization reaction, the pore structure still existed after the coating. The element distribution proved that the sulfonation reaction was homogeneous and the PANI was coated onto the PS evenly (Fig. 4).

3.2. The adsorption property of porous PANI/PS for Sr^{2+}

3.2.1. The effect of pH

The effect of pH on the adsorption capacity of Sr^{2+} was studied in the pH range of 1.0–10.0 for Sr^{2+}, as shown in Fig. 5a. One can see that the adsorption of Sr^{2+} on porous PANI/PS dramatically enhanced with increasing pH from 1.0 to 5.0, and then remained the high-level adsorption at pH > 5.0. It was reported that Sr^{2+} was the predominant species within the pH range of 1.0–10.0 [48]. Therefore, the change of adsorption capacity with increasing the pH can be inferred as the change of the surface properties of porous PANI/PS. The final pHs of the adsorption solution also had been recorded after the adsorption process (Fig. 5a). We found that the final pH increased with the increase of the pH from 1.0 to 5.0 and remained in the range of 5.0–10.0. The essential reason was the interaction of between the PANI and the H^+. It also can be evidenced by zeta potentials of porous PANI/PS in different pH solution (Fig. 5b). Clearly, the PANI/PS still had electronegativity in the measured range of pH, and the zeta potential decreased gradually with increasing the pH. At low pH (1.0–4.0), the porous PANI/PS had less negative charge, because of the protonation reaction. At high pH (5.0–10.0), the concentration of deprotonated sites increased with increasing pH, because of the surface deprotonation reaction. The deprotonated sites were more available to retain the positively charged Sr^{2+}, and more adsorption sites were available for binding Sr^{2+} on porous PANI/PS, thus resulting in an increase of Sr^{2+} adsorption.

3.2.2. The effect of initial concentration

The effect of initial concentration on the adsorption capacity is illustrated in Fig. 5c. Clearly, the adsorption capacity rapidly increased with increasing the initial concentration of Sr^{2+} in the range of 0–100 mg/L. The Sr^{2+} uptake of the porous PANI/PS increased rapidly when the concentration of Sr^{2+} was lower than 50 mg/L, and then

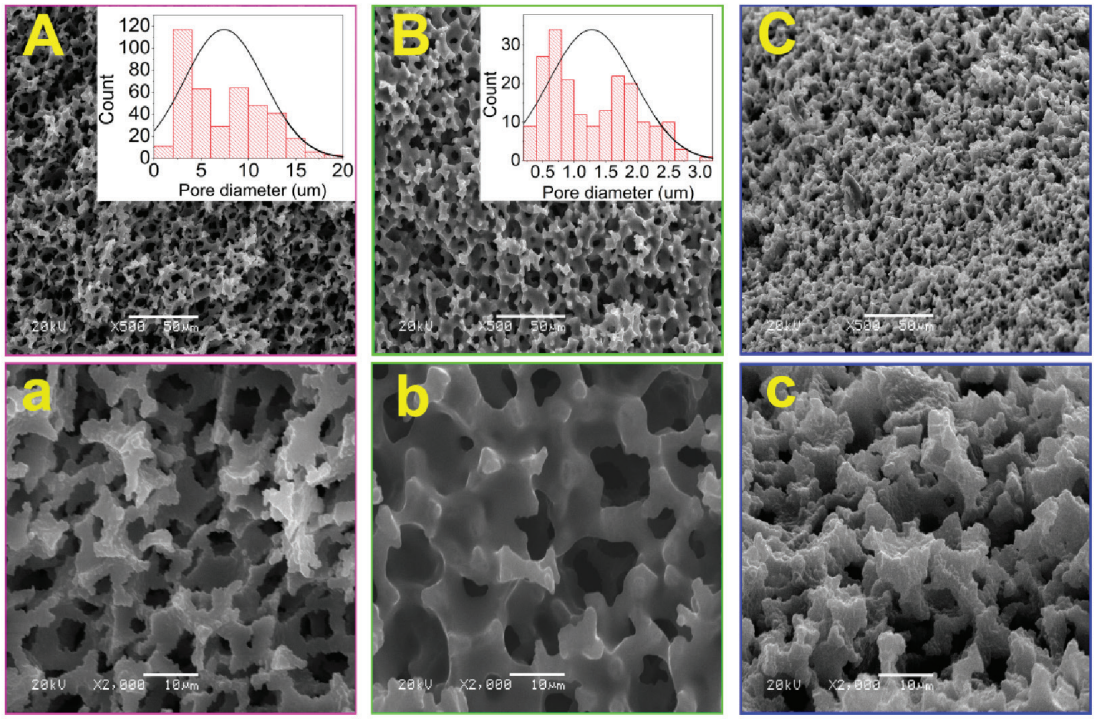

Fig. 3. SEM of porous PS (A, a), sulfonated PS (B, b) and PANI/PS (C, c). The scale bars were 50 μm for A, B, C and 10 μm for a, b, c, respectively.

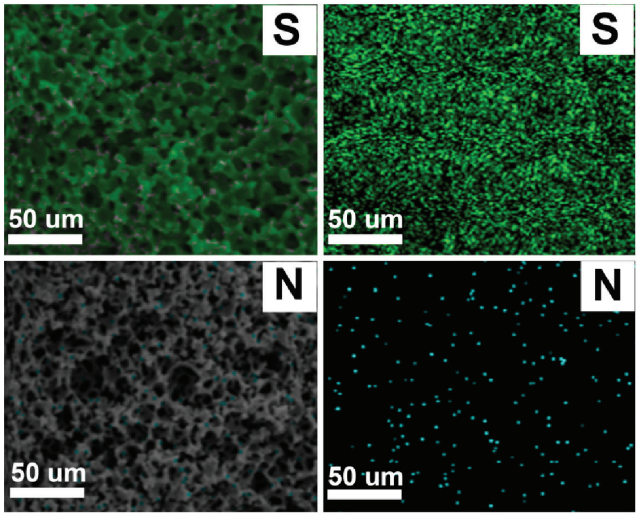

Fig. 4. The elements distribution of S in sulfonated PS and N in porous PANI/PS.

remained a constant value when the Sr^{2+} concentration exceeded 100 mg/L. At that time, the adsorption equilibrium was reached and all the adsorption sites had been occupied by Sr^{2+}. The reason was that the driving force at the solid–liquid interface (ion exchange, electrostatic attraction and chelation) was increased with increasing the initial ion concentration, which was benefit for enhancing the adsorption holding and capacities of the adsorbent for metal ions. The maximum adsorption capacity of the PANI/PS was 58.85 mg/g, which was higher than the sulfonated PS of 36.97 mg/g. It was indicated that the benzenoid diamine nitrogen had strong affinity with Sr^{2+}.

In order to demonstrate the adsorption mechanism, two isotherms models of Langmuir and Freundlich models were used for the study of the adsorption mechanism. Langmuir isotherm model was applicable for the monolayer absorption and sorption occurred only on localized sites and involves no interactions between adsorbed molecules. Freundlich adsorption model was applied to adsorption onto heterogeneous surfaces with a uniform energy distribution. The linear equations are expressed as [49,50]:

Langmuir isotherm model:

$$C_e/q_e = C_e/Q_m + 1/(Q_m \times K_L) \quad (2)$$

Freundlich isotherm model:

$$\text{Log } q_e = \log K_F + 1/n \times \log C_e \quad (3)$$

where C_e (mg/L) and q_e (mg/g) were the equilibrium concentration and equilibrium adsorption capacity at certain initial concentration, respectively. Q_m (mg/g) was the maximum adsorption capacity. K_L (L/mg) and K_F ($mg^{1-1/n}$ $L^{1/n}$/g) were the isotherm constants for Langmuir isotherm

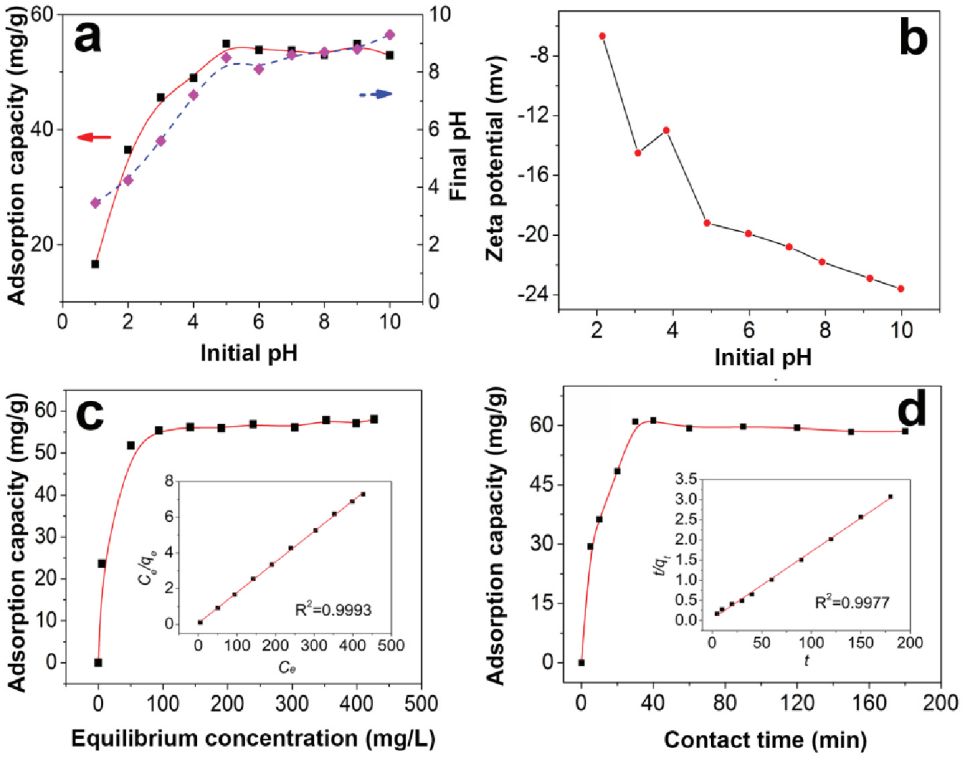

Fig. 5. The effect of solution pH on the adsorption of Sr^{2+} (a), the zeta potential of porous PANI/PS in different pH solution (b), the effect of the initial concentration (c) and the contact time (d) on the adsorption of Sr^{2+}. The interpolated images of in Figs. 4c and 4d were the fitting curve of the Langmuir isotherm model and pseudo-second-order model, respectively. Adsorption conditions: sample dose: 20 mg/25 mL; initial concentration: 100 mg/L; temperature: 30°C.

and Freundlich isotherm, which can be determined by linear regression of the experimental data, and n (dimensionless) was the constant depicting the adsorption intensity. The estimated model parameters with correlation coefficient (R^2) are listed in Table 1.

Based on Table 1, it can be seen that the Langmuir isotherm model was expected to be suitable for describing the adsorption of porous PANI/PS for Sr^{2+}. In addition to higher correlation coefficients (R), the adsorption capacity calculated from the Langmuir isotherm model was closer to the experimental data, suggesting that the sorption of Sr^{2+} occurred on the surface of PANI/PS was monolayer and the adsorption sites loaded on the porous PS was homogeneous.

Comparisons of adsorption capacity between the referenced adsorbents and the porous adsorbent prepared in this study are summarized in Table 2. The comparative results demonstrated that this porous PANI/PS adsorbent showed higher adsorption capacity than other adsorbents reported for Sr^{2+}, except for the ordered mesoporous carbon. The efficient adsorption property was attributed to the sufficient porous structure and abundant functional groups in the PANI/PS.

3.2.3. The effect of contact time

Equilibrium time was one of the important factors to evaluate the application potential of a synthetic material in water treatment. It was clear that the adsorption capacity increased rapidly in the first 10 min, and the equilibrium was achieved within 30 min (Fig. 5d). This illustrated that the porous structure was favorable for the diffusion of Sr^{2+} into the matrix of the porous PS. The Sr^{2+} in the aqueous solution can easily enter into the pore channels and diffuse quickly across the internal and external surface of PANI/PS. In order to guarantee the adsorption of Sr^{2+} on porous PANI/PS completely, 1 h was selected as the shaking time in the following experiment.

The kinetic adsorption data were simulated with two dynamic models of pseudo-first-order, pseudo-second-order model to analyze the adsorption process. The equation was expressed as:

Pseudo-first-order model:

$$\log (q_e - q_t) = \log q_e - (k_1/2.303) \times t \quad (4)$$

Pseudo-second-order model:

$$t/q_t = 1/k_2 q_e^2 + t/q_e \quad (5)$$

Table 1
The constant parameters and correlation coefficients of Langmuir model and Freundlich model for Sr^{2+} adsorption onto the adsorbent

$q_{e,exp}$ (mg/g)	Langmuir isotherm model		Freundlich isotherm model	
58.85	Q_m (mg/g)	58.85	K_F	49.77
	K_L (L/mg)	2.42×10^{-1}	n	39.84
	R_L^2	0.9993	R_F^2	0.9262

Table 2
Comparison of Sr^{2+} adsorption among different adsorbents

Adsorbent	Adsorption condition	Adsorption capacity (mg/g)	Reference
Sericite	m/v = 2.0 g/L, pH = 3.0	21.41	[51]
Na-rectorite	m/V = 0.6 g/L	14.28	[52]
Alginate microsphere	m/v = 2.0 g/L	41.0	[53]
Grapheme oxide–magnetite	m/V = 2.0 g/L, pH = 6.5	22.3	[54]
Polyacrylamide modified graphene oxide composites	m/V = 0.2 g/L, pH = 5.5	27.84	[55]
Ordered mesoporous carbon	m/V = 5 g/L, pH = 6.0	7.3	[56]
Green geopolymer/alginate hybrid spheres	m/V = 2 g/L, pH = 6.74	12.59	[57]
Porous PANI/PS	m/V = 0.8 g/L, pH = 6.0	58.85	In this study

where q_t (mg/g) was the amount adsorbed for Sr^{2+} at the time t, and the q_e (mg/g) was the equilibrium absorption capacity, k_1 (min^{-1}) and k_2 (g/mg·min) were the rate constant of pseudo-first-order equation and pseudo-second-order equation, respectively. The simulated results are listed in Table 3. A comparison of the correlation coefficients (R^2) of pseudo-first-order and pseudo-second-order model, the pseudo-second-order model simulated the kinetic data better than pseudo-first-order model. It was indicated that the adsorption of Sr^{2+} onto the porous PANI/PS may be chemisorptions rather than mass transport.

3.2.4. Regeneration and reusability

The adsorbent with better regeneration capacity and recovery capacity for metal ions was desirable from the viewpoint of usage cost and recovery of value metals. The reusability of magnetic porous PANI/PS was evaluated via six consecutive adsorption-desorption cycles. As shown

Table 3
Estimated adsorption kinetic parameters for Sr^{2+} by pseudo-first-order and pseudo-second-order model

$q_{e,exp}$(mg/g)	Pseudo-first-order		Pseudo-second-order	
58.85	$q_{e,cal}$ (mg/g)	2.71	$q_{e,cal}$ (mg/g)	60.24
	k_1(min^{-1})	3.91×10^{-3}	k_1(g/mg·min)	6.09×10^{-3}
	R_1^2	0.0106	R_2^2	0.9977

in Fig. 6, the PANI/PS still kept the intact shape without any breakage in the solution after six cycles (Fig. 6a), and the PANI/PS can be separated easily from the solution by using a tweezer (Figs. 6b,c), indicating that the PANI/PS had strong mechanical strength. Besides, with increasing the adsorption–desorption cycles, the adsorption capacity of Sr^{2+} only showed a slightly decrease. And the adsorption capacity still reached as high as 53.68 mg/g for Sr^{2+} after six times of sorption, demonstrating that the as-prepared porous PANI/PS monolith was recyclable adsorbents for Sr^{2+} removal with high-performance (Fig. 6d).

3.3. The adsorption mechanism

The Sr^{2+} removal mechanism by porous PANI/PS adsorbent was explored by FTIR spectra (Fig. 7). The dried samples before and after adsorption of Sr^{2+} were compared. The peaks at 1297 cm^{-1} and 1124 cm^{-1} corresponding to C–N stretching vibration and C=N stretching vibration in the spectrum shifted to 1301 cm^{-1} and 1127 cm^{-1} after sorption of Sr^{2+}, respectively. Besides, the peak at the 1597 cm^{-1} assigned as C=C in benzenoid rings of PANI shifted to 1594 cm^{-1}. All these informations indicated that the amino groups were involved in the sorption process.

The XPS was frequently used to distinguish the different forms of the same element and explore the adsorption mechanism. Fig. 8 showed the XPS spectra of the porous PANI/PS before and after the adsorption. It was obvious that the Sr 3d peak appeared in the spectra of the porous PANI/PS after the adsorption, indicating that the Sr^{2+} was adsorbed onto the porous PANI/PS. The peaks of N 1s at 398.5 eV and 399.6 eV corresponded to quinoid di-imine nitrogen (–N=) and benzenoid diamine

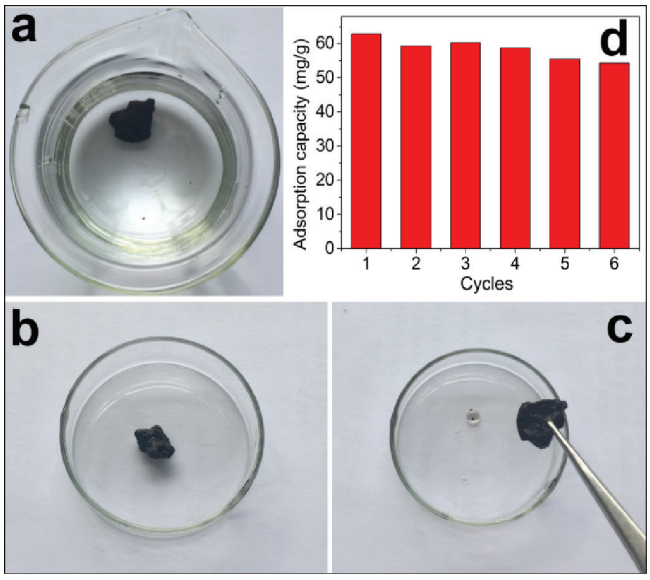

Fig. 6. The digital photograph of the PANI/PS in the solution (a) or in a culture dish (b) after six adsorption-desorption cycles, and pick up the PANI/PS by using tweezers (c), the amount adsorbed for Sr^{2+} as a function of adsorption-desorption cycle (d). Adsorption time: 1 h; adsorption dose: 20 mg/25 mL; desorption time: 1 h; 30°C/120 rpm.

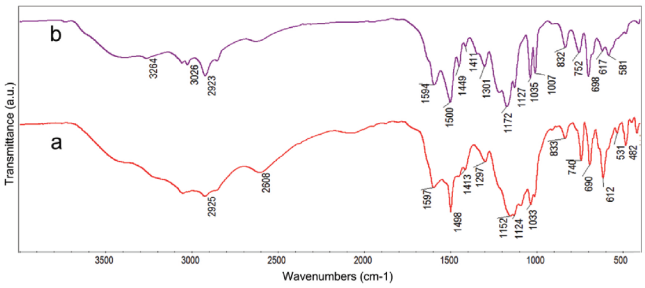

Fig. 7. FTIR spectra of porous PANI/PS adsorbent before (a) and after adsorption of Sr^{2+} (b).

nitrogen (–NH–), respectively. The peaks at 401.1 eV and 401.9 eV can be ascribed to positive charged nitrogen: oxidized amine and protonated imine, respectively [58]. Compared the peaks of N 1s before and after adsorption, the original PANI/PS had a higher proportion of positive charged nitrogen. The reason may be caused by the acidic reaction environment during the preparation process of PANI/PS. When the PANI/PS was used to adsorb the Sr^{2+} in the solution, the deprotonation reaction accelerated due to the facts that the pH of Sr^{2+} solution was close to neutralization (pH = 6). Besides, the peak of benzenoid

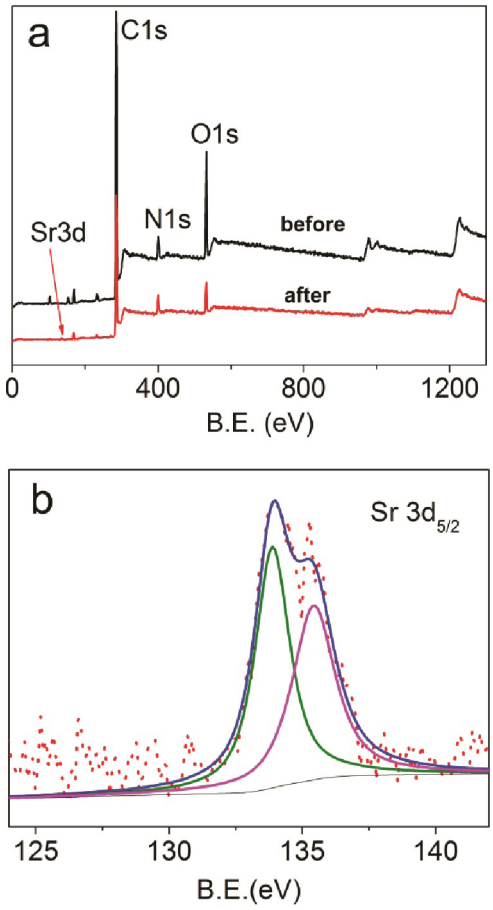

Fig. 8. XPS spectra, Sr 3d and N 1s spectra of the porous PANI/PS before (c) and after (d) adsorption of Sr^{2+}.

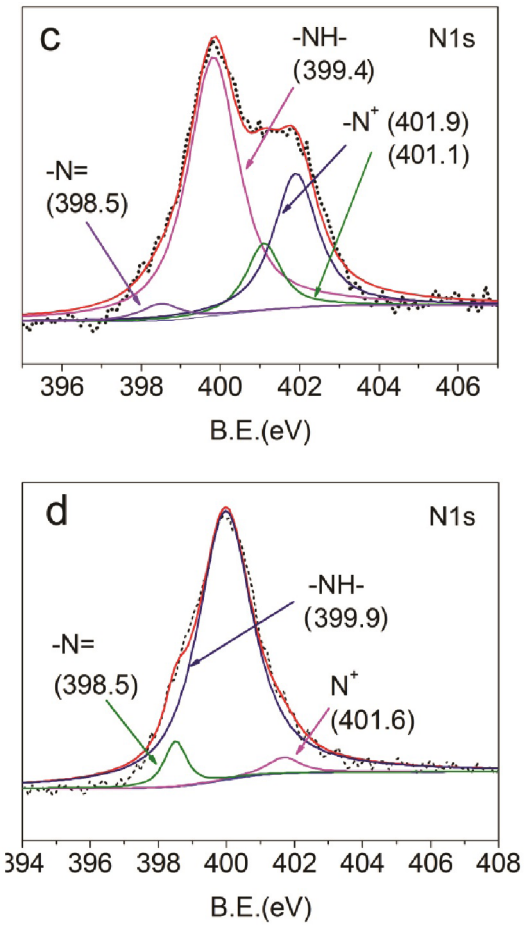

Fig. 8. XPS spectra, Sr 3d and N 1s spectra of the porous PANI/PS before (c) and after (d) adsorption of Sr^{2+}.

diamine nitrogen (–NH–) slightly shifted from 399.4 to 399.9 eV after the adsorption process, confirming that the benzenoid diamine nitrogen could form surface complexes with Sr^{2+}.

4. Conclusions

The porous PS with sufficient pore structure was firstly prepared from the W/O HIPEs and then a novel monolithic porous adsorbent of PANI/PS was prepared by coating the PANI onto the surface of porous PS. The FTIR and SEM analysis results showed that the porous morphology of PANI/PS changed obviously as compared with the porous PS. The as-prepared porous adsorbent had fast adsorption kinetics and stronger adsorption ability for Sr^{2+} in the pH range of 5.0–10.0. The adsorption process was reasonably correlated with the pseudo second-order model and the Langmuir isotherm model. Six consecutive adsorption-desorption processes demonstrated that the adsorbent showed excellent desorption performance and reusability for Sr^{2+}. Hence, the prepared porous PANI/PS showed a promising potential for Sr^{2+} recovery from the relative wastewater resources.

Acknowledgments

This work was supported by the National Natural Science Foundation of China (21706267 and U1407114) for the financial support for this research.

References

[1] D. Sriranganathan, X. Chen, K.A. Hing, N. Kanwald, R.G. Hill, The effect of the incorporation of fluoride into strontium containing bioactive glasses, J. Non–Cryst. Solids., 457 (2017) 25–30.
[2] H.H. Nguyen, F. Milat, P.R. Ebeling, A new contralateral atypical femoral fracture despite sequential therapy with teriparatide and strontium ranelate, Bone Rep., 6 (2017) 34–37.
[3] M.J. Iqbal, S. Farooq, Could binary mixture of Nd–Ni ions control the electrical behavior of Strontium barium M–type hexaferrite nanoparticles, Mater. Res. Bull., 46 (2011) 662–667.
[4] M. Jamalian, A. Ghasemi, E.A. Paimozd, Comparison of the magnetic and microwave absorption properties of Mn–Sn–Ti substituted strontium ferrite with and without multi-walled carbon nanotube, Curr. Appl. Phys., 14, (2014) 909–915.
[5] S. Taylor, A. Samokhvalov, Water as probe molecule for midgap states in nanocrystalline strontium titanate by conventional and synchronous luminescence spectroscopy under ambient conditions, Spectrochim. Acta A, 174 (2017) 54–61.
[6] A. Sachse, A. Merceille, Y. Barré, A. Grandjeanc, F. Fajula, A. Galarneau, Macroporous LTA-monoliths for in-flow removal of radioactive strontium from aqueous effluents: application to the case of Fukushima, Microporous Mesoporous Mater., 164 (2012) 251–258.
[7] Z. Cheng, Z. Gao, W. Ma, Q. Sun, B. Wang, X. Wang, Preparation of magnetic Fe_3O_4 particles modified sawdust as the adsorbent to remove strontium ions, Chem. Eng. J., 209 (2012) 451–457.
[8] W. Mu, Q. Yu, X. Li, H. Wei, Y. Jian, Niobate nanofibers for simultaneous adsorptive removal of radioactive strontium and iodine from aqueous solution, J. Alloy. Compd., 693 (2017) 550–557.
[9] C. Xu, J. Wang, J. Chen, Solvent extraction of strontium and cesium: a review of recent progress, Solvent Extr. Ion Exch., 30 (2012) 623–650.
[10] I.M. El-Naggar, G.M. Ibrahimm, B. EL-Gammal, E.A. El-Kady, Integrated synthesis and characterization of some porous polyacrylamide-based composites for cationic sorption from aqueous liquid wastes, Desal. Water Treat., 52 (2014) 6802–6816.
[11] A.F. Shaaban, T.Y. Mohamed, D.A. Fadel, N.M. Bayomi, Removal of Ba(II) and Sr(II) ions using modified chitosan beads with pendent amidoxime moieties by batch and fixed bed column methods, Desal. Water Treat., 82 (2017) 131–145.
[12] H. Hye-Jin, K. Byoung-Gyu, H. Jeongsik, Enhanced Sr adsorption performance of MnO_2–alginate beads in seawater and evaluation of its mechanism, Chem. Eng. J., 319 (2017) 163–169.
[13] W. Mu, Q. Yu, X. Li, Efficient removal of Cs^+ and Sr^{2+} from aqueous solution using hierarchically structured hexagonal tungsten trioxide coated Fe_3O_4, Chem. Eng. J., 319 (2017) 170–178.
[14] S.M. Al-Jubouri, N.A. Curry, S.M. Holmes, Hierarchical porous structured zeolite composite for removal of ionic contaminants from waste streams and effective encapsulation of hazardous waste, J. Hazard. Mater., 320 (2016) 241–251.
[15] J. Ryu, S. Kim, H.J. Hong, J. Hong, M. Kim, T. Ryu, I.S. Park, K.S. Chung, J.S. Jang, B.G. Kim, Strontium ion (Sr^{2+}) separation from seawater by hydrothermally structured titanate nanotubes: removal vs. recovery, Chem. Eng. J., 304 (2016) 503–510.
[16] L. Zhang, J.Wei, X. Zhao, F. Li, F. Jiang, M. Zhang, X. Cheng, Removal of strontium (II) and cobalt (II) from acidic solution by manganese antimonite, Chem. Eng. J., 302 (2016) 733–743.

[17] A. Rengaraj, Y. Haldora, P. Puthiaraj, S.K. Hwang, T. Ryu, J. Shin, Y.S. Huh, Covalent triazine polymer–Fe_3O_4 nanocomposite for strontium ion removal from seawater, Ind. Eng. Chem. Res., 56 (2017) 4984–4992.
[18] V. Srivastava, P. Maydannik, M. Sillanpää, Synthesis and characterization of PPy@ NiO nano-particles and their use as adsorbent for the removal of Sr (II) from aqueous solutions, J. Mol. Liq., 223 (2016) 395–406.
[19] L.Y. Zhang, W. Zhang, Z. Zhou, C.M. Li, γ–Fe_2O_3 nanocrystals-anchored macro/meso-porous graphene as a highly efficient adsorbent toward removal of methylene blue, J. Colloid Interface Sci., 476 (2016) 200–205.
[20] A. Gignone, M. Delle Piane, M. Corno, P. Ugliengo, B. Onida, Simulation and experiment reveal a complex scenario for the adsorption of an antifungal drug in ordered mesoporous silica, J. Phys. Chem. C, 119 (2015) 13068–13079.
[21] N. Guo, S. Su, B. Liao, S. Ding, W. Sun, Preparation and properties of a novel macro porous Ni^{2+}–imprinted chitosan foam adsorbents for adsorption of nickel ions from aqueous solution, Carbohyd. Polym., 165 (2017) 376–383.
[22] X. Zhang, B. Gao, A.E. Creamer, Adsorption of VOCs onto engineered carbon materials: A review, J. Hazard. Mater., 338 (2017) 102–123.
[23] E. Rangel-Range, J. Weber, J.G. de la Campa, M. Iglesias, E.M. Maya, Pluronic-assisted hydrothermal synthesis of microporous polyimides. Application as supports for heterogenized transition metal catalysts, Microporous Mesoporous Mater., 239 (2017) 287–295.
[24] D.F. Izquierdo, M. Yates, P. Lozano, M.I. Burguete, E. García-Verdugo, S.V. Luis, Macroporous polymers tailored as supports for large biomolecules: Ionic liquids as porogenic solvents and as surface modifiers, React. Funct. Polym., 85 (2014) 20–27.
[25] Z. Jia, Q. Wang, D. Ren, R. Zhu, Fabrication of one-dimensional mesoporous α–Fe_2O_3 nanostructure via self-sacrificial template and its enhanced Cr (VI) adsorption capacity, Appl. Surf. Sci., 264 (2013) 255–260.
[26] A. Quell, T. Sottmann, C. Stubenrauch, Diving into the finestructure of macroporous polymer foams synthesized via emulsion templating: A phase diagram study, Langmuir, 33 (2017) 537–542.
[27] M.S. Silverstein, PolyHIPEs: Recent advances in emulsion-templated porous polymers, Prog. Polym. Sci., 39 (2014) 199–234.
[28] Y. Zhu, Y. Zheng, L. Zong, F. Wang, A. Wang, Fabrication of magnetic hydroxypropyl cellulose-g-poly(acrylic acid) porous spheres via Pickering high internal phase emulsion for removal of Cu^{2+} and Cd^{2+}, Carbohyd. Polym., 149 (2016) 242–250.
[29] M. Wickenheisser, T. Paul, C. Janiak, Prospects of monolithic MIL–MOF@poly(NIPAM)HIPE composites as water sorption materials, Microporous Mesoporous Mater., 220 (2016) 258–269.
[30] E.H. Mert, H. Yıldırım, A.T. Üzümcü, H. Kavas, Synthesis and characterization of magnetic polyHIPEs with humic acid surface modified magnetic iron oxide nanoparticles, React. Funct. Polym., 73 (2013) 175–181.
[31] Y. Zhu, W. Wang, Y. Zheng, F. Wang, A. Wang, Rapid enrichment of rare-earth metals by carboxymethyl cellulose-based open-cellular hydrogel adsorbent from HIPEs template, Carbohyd. Polym., 140 (2016) 51–58.
[32] J. Pan, Q. Qu, J. Cao, D. Yan, J.X. Liu, X.H. Dai, Molecularly imprinted polymer foams with well-defined open-cell structure derived from Pickering HIPEs and their enhanced recognition of λ-cyhalothrin, Chem. Eng. J., 253 (2014) 138–147.
[33] J. Pan, Y. Ma, J. Zeng, X.H. Niu, T. Zhang, F.X. Qiu, Y.S. Yan, Facile assembly of hollow polydopamine capsules onto macroporous poly(glycidyl methacrylate) foams for simultaneous removal of λ-cyhalothrin and copper ions, Chem. Eng. J., 302 (2016) 670–681.
[34] F. Saadati, M. Rahmani, F. Ghahramani, Synthesis of a novel ion-imprinted polyaniline/hyper-cross-linked polystyrene nanocomposite for selective removal of lead(II) ions from aqueous solutions, Desal. Water Treat., 82 (2017) 210–218.
[35] B. Qiu, C. Xu, D. Sun, Q. Wang, H.B. Gu, X. Zhang, Z.H. Guo, Polyaniline coating with various substrates for hexavalent chromium removal, Appl. Surf. Sci., 334 (2015) 7–14.
[36] A. Alshameri, C. Yan, X. Lei, Enhancement of phosphate removal from water by TiO_2/Yemeni natural zeolite: preparation, characterization and thermodynamic, Microporous Mesoporous Mater., 196 (2014) 145–157.
[37] Y. Gao, C. Chen, X. Tan, H. Xu, K.R. Zhu, Polyaniline-modified 3D-flower-like molybdenum disulfide composite for efficient adsorption/photocatalytic reduction of Cr(VI), J. Colloid Interface Sci., 476 (2016) 62–70.
[38] B. Mu, J. Tang, L. Zhang, A.Q. Wang, Preparation, characterization and application on dye adsorption of a well-defined two-dimensional superparamagnetic clay/polyaniline /Fe_3O_4 nanocomposite, Appl. Surf. Sci., 132–133 (2016) 7–16.
[39] X. Liu, C. Cheng, C. Xiao, D.D. Shao, Z.M. Xu, J.Q. Wang, W.J. Wang, Polyaniline (PANI) modified bentonite by plasma technique for U(VI) removal from aqueous solution, Appl. Surf. Sci., 411 (2017) 331–337.
[40] M.A. Salem, R.G. Elsharkawy, M.F. Hablas, Adsorption of brilliant green dye by polyaniline/silver nanocomposite: Kinetic, equilibrium, and thermodynamic studies, Eur. Polym. J., 75 (2016) 577–590.
[41] Q. Zhou, Y. Wang, J. Xiao, H. Fan, Adsorption and removal of bisphenol A, α-naphthol and β-naphthol from aqueous solution by Fe_3O_4@polyaniline core–shell nanomaterials, Synth. Met., 212 (2016) 113–122.
[42] R. Karthik, S. Meenakshi, Removal of Cr(VI) ions by adsorption onto sodium alginate-polyaniline nanofibers, Int. J. Biol. Macromol., 72 (2015) 711–717.
[43] K. Zarrini, A.A. Rahimi, F. Alihosseini, H. Fashandi, Highly efficient dye adsorbent based on polyaniline-coated nylon–6 nanofibers, J. Clean. Prod., 142 (2017) 3645–3654.
[44] S. Bhattarai, J.S. Kim, Y.S. Yun, Y.S. Lee, Preparation of polyaniline-coated polystyrene nanoparticles for the sorption of silver ions, React. Funct. Polym., 105 (2016) 52–59.
[45] O. Ozer, A. Ince, B. Karagoz, N. Bicak, Crosslinked PS-DVB microspheres with sulfonated polystyrene brushes as new generation of ion exchange resins, Desalination, 309 (2013) 141–147.
[46] X. Hu, Y. Zhang, K. Tang, G.L. Zou, Hemoglobin-biocatalysts synthesis of a conducting molecular complex of polyaniline and sulfonated polystyrene, Synth. Met., 150 (2005) 1–7.
[47] A.M. Youssef, S.A. Mohamed, M.S. Abdel-Aziz, M.E. Abdel-Aziz, G. Turky, S. Kamel, Biological studies and electrical conductivity of paper sheet based on PANI/PS/Ag–NPs nanocomposite, Carbohyd. Polym., 147 (2016) 333–343.
[48] Y. Sun, X. Wang, C. Ding, W. Cheng, C. Chen, T. Hayat, X. Wang, Direct synthesis of bacteria-derived carbonceous nanofibers as a highly efficient material for radionuclides elimination, ACS Sustain. Chem. Eng., 4 (2016) 4608–4616.
[49] R.M. Ali, H.A. Hamad, M.M. Hussein, G.F. Malash, Potential of using green adsorbent of heavy metal removal from aqueous solutions: adsorption kinetics, isotherm, thermodynamic, mechanism and economic analysis, Ecol. Eng., 91 (2016) 317–332.
[50] T.M. Mutuvari, C.D. Tran, Synergistic adsorption of heavy metal ions and organic pollutants by supramolecular polysaccharide composite materials from cellulose, chitosan and crown ether, J. Hazard. Mater., 264 (2014) 449–459.
[51] B. Hu, Q. Hu, D. Xu, C. Chen, Macroscopic and microscopic investigation on adsorption of Sr(II) on sericite, J. Mol. Liq., 225 (2017) 563–568.
[52] Y. Zhao, Z. Shao, C. Chen, J. Hu, H. Chen, Effect of environmental conditions on the adsorption behavior of Sr(II) by Na-rectorite, Appl. Clay Sci., 87 (2014) 1–6.
[53] H. Hong, J. Ryu, I. Park, T. Ryu, K. Chung, B. Kim, Investigation of the strontium (Sr(II)) adsorption of an alginate microsphere as a low-cost adsorbent for removal and recovery from seawater, J. Environ. Manage., 165 (2016) 263–270.

[54] A. Tayyebi, M. Outokesh, S. Moradi, A. Doram, Synthesis and characterization of ultrasound assisted "graphene oxide–magnetite" hybrid, and investigation of its adsorption properties for Sr(II) and Co(II) ions, Appl. Surf. Sci., 353 (2015) 350–362.
[55] H. Qi, H. Liu, Y. Gao, Removal of Sr(II) from aqueous solutions using polyacrylamide modified graphene oxide composites, J. Mol. Liq., 208 (2015) 394–401.
[56] Y. Song, G. Ye, J. Chen, D. Lv, J. Wang, Wet oxidation of ordered mesoporous carbon FDU–15 by using $(NH4)_2S_2O_8$ for fast adsorption of Sr(II): An investigation on surface chemistry and adsorption mechanism, Appl. Surf. Sci., 357 (2015) 1578–1586.
[57] Z. Cheng, Z. Gao, W. Ma, Q. Sun, B. Wang, X. Wang, Preparation of magnetic Fe_3O_4 particles modified sawdust as the adsorbent to remove strontium ions, Chem. Eng. J., 209 (2012) 451–457.
[58] S. Golczak, A. Kanciurzewska, M. Fahlman, K. Langer, J.J. Langer, Comparative XPS surface study of polyaniline thin films, Solid State Ionics, 179 (2008) 2234–2239.